Experimental Investigation and Model Development for Effective Viscosity of MgO-Ethylene Glycol Nanofluids by using Dimensional Analysis, FCM-ANFIS and GA-PNN Techniques

Saheed Adewale Adio, Mehdi Mehrabi, Mohsen Sharifpur[1] and Josua Petrus Meyer

Department of Mechanical and Aeronautical Engineering, University of Pretoria, Pretoria 0002, South Africa.

Abstract

Desirable effective viscosity behaviour is an essential transport property required for the effective utilisation of nanofluids in industrial systems as well as other applications. Viscosity influences significantly the pumping power and heat transfer effectiveness in a thermal system since Reynolds and Prandtl numbers are functions of viscosity. In this study, the optimum energy required for the preparation of MgO-ethylene glycol (MgO-EG) nanofluids was determined by varying the ultrasonication energy input into the preparation process. The uniformly dispersed nanofluids were characterised and the viscosity measurements were carried out as a function of temperature (20 to 70 ^{o}C), nanoparticle volume fraction (0 to 5%) and nanoparticles size (~21, ~105 and ~125 nm). Based on the experimental data, the effective viscosity of all the samples irrespective of nanoparticle size or volume fraction, decreases exponentially with increase in temperature and the trend is similar to that of the base fluid, but in different magnitude. Increasing the volume fraction of the MgO nanoparticles showed a corresponding increase in the effective viscosity of the nanofluid. It was also noticed that the samples containing 21 nm MgO showed higher effective viscosity compared to samples containing 105 and 125 nm MgO when the volume fraction is constant. The viscosity values in the present study quite differ from the values predicted by the existing prominent viscosity models as well as the existing models do not consider all the variables of present data (temperature, nanoparticle volume fraction and nanoparticles size). Therefore, new correlation is proposed using the method of dimensional analysis and considering essential factors, including nanoparticle size, volume fraction temperature, capping layer thickness, viscosity of the base fluid, the density of base fluid and the density of nanofluid as input parameters. Furthermore, genetic algorithm-polynomial neural network (GA-PNN) and fuzzy C-means clustering-based adaptive neuro-fuzzy inference system (FCM-ANFIS) was used to model the effective viscosity of the MgO-EG nanofluids considering the parameters mentioned above. The results of all the modelling techniques showed good agreement with the experimental data.

Keywords: Nanofluid, effective viscosity, MgO-ethylene glycol, GA-PNN, FCM-ANFIS

[1] E-mail: Mohsen.Sharifpur@up.ac.za (M. Sharifpur)

Tel: +27 12 420 2448

1. Introduction

In recent times, energy efficient systems have shared features which are portability, compactness and lightness in weight. These systems, such as mobile electronics, microelectromechanical systems (MEMs), nanoelectromechanical systems (NEMs) and power generating systems/devices are commonly used in major industries such as the electronics, energy, and transportation. Moreover, these systems are designed to perform more efficiently and have higher throughput than the previous systems which are massive, non-portable and heavy. The ratio of the increased throughput/efficiency to size is accompanied with thermal management challenges due to their high power density. The classic methods of improving heat transfer include an increase in heat transfer surface area (adding fins) and/or increasing convective heat transfer coefficient which they both have limitations. Other emerging methods such as geometric optimization of heat exchangers and the use of functionally graded materials, also have major setbacks. For instance, using extended surface increases the bulkiness of heat exchangers which contradicts the new design philosophy of attaining sustainable development and global energy sustainability. On the other hand, the use of functionally graded materials raises economic concerns because of the high price of functionally graded materials.

Nanofluid is a modified heat transfer fluid produced by homogenizing nanoparticles in conventional heat transfer fluids such as water or ethylene glycol (EG). Research findings have shown that nanofluids have improved thermal properties such as thermal conductivity, heat capacity and convective heat transfer coefficient [1, 2]. Heat transfer fluid that possesses higher thermal conductivity provides better heat removal capacity and also could support the reduction of the size and weight of heat exchanger in line with the global sustainable development and energy sustainability. Therefore, as the next-in-line heat transfer fluid, nanofluid has received a considerable interest from the time when its thermal properties were first reported. Eastman et al. [3] investigated the thermal conductivity of Cu-EG nanofluids. They dispersed Cu nanoparticles having a mean diameter less than 10 nm in EG using a single-step procedure. Their results showed up to 40% enhancement in thermal conductivity of the Cu-EG nanofluid compared to the base fluid (EG) for a Cu volume fraction of 0.3% and thioglycolic acid was used as a pH modifier in order to improve the stability of the Cu-EG nanofluids. Kang et al. [4] showed that the enhancement obtainable from the dispersion of ultra-dispersed diamond nanoparticles (UDD) with 30-50 nm size in EG was up to 50% at 1% volume fraction. They also showed that for 8-15 nm silver (Ag) dispersed in water at 0.4% volume fraction, there was enhancement of 10% in thermal conductivity. Similar results for other types of nanofluids were reported by Murshed et al. [5] and Das et al. [6].

The presence of particles in a fluid medium creates increased resistance to flow of nanofluids due to intensified energy dissipation rate arising from the interactions between the particles and particle-fluid. Therefore, the problem of viscosity increase with an increase in the suspended volume fraction of nanoparticles is a major challenge that requires extensive investigations experimentally, besides, there exist the lack of models that can accurately predict the viscosity of nanofluids. If this problem is not properly understood and tackled, it may diminish the efficacy of nanofluids in practical applications [7].

In the past, the influence of nanoparticles dispersion on the viscosity of nanofluids has been investigated for some nanofluids as summarised below. Chandrasekar et al. [8] used microwave assisted technique to synthesise Al_2O_3 nanoparticles having an average particle size (APS) of 43 nm. They dispersed 0.33 to 5% volume fractions of the Al_2O_3 in deionized water (DI-water) and investigated their viscosity enhancement at room temperature. Their results showed a staggering viscosity increase of 136% at the suspension of 5% Al_2O_3. Fedele et al. [9] investigated the effective viscosity of DI-water based TiO_2 nanofluid with TiO_2 % weight between 1 to 35 %wt and temperature range of 10-70 ^oC. They also observed a very high viscosity increase of 243% at 35 %wt of TiO_2 suspended.

To improve the viscosity of nanofluids, stability of nanoparticles in the base fluid must be ensured and there are about three effective methods that have been used viz: (i) addition of surfactant (ii) pH modification (iii) ultrasonic vibration. Timefeeva et al. [10] showed that modifying the pH of α-SiC/water nanofluid provided good stability for the 29 nm SiC nanoparticles in the base fluid and eventual reduction in the effective viscosity up to 34%. Zhao et al. [11] also observed that the viscosity of SiO_2-water nanofluid is significantly influenced by the pH value of the suspension. Li et al. [12] stabilised 25 nm Cu-water nanofluids using pH and/or sodium dodecylbenzensulfonate (SBDS) chemical surfactant. Although, they only measured thermal conductivity, the influence of surfactant was such that it reduced the nanoparticles agglomerate size when applied in right proportion [13]. Song and Youn [14] showed that poor dispersion can increase the effective viscosity of carbon nanotube (CNT)-epoxy nanocomposite and as a result, they used ultrasonic vibration to aid proper dispersion and minimise viscosity enhancement. Yang et al. [13] varied the energy of ultrasonication applied to the dispersion of multiwall carbon nanotubes (MWCNTs) in poly (α-oleifin) oil in order to obtain proper homogenisation of the MWCNTs at which point the viscosity was minimised.

A good nanofluid is supposed to have high thermal conductivity to be very efficient in thermal management (heat removal), and minimum viscosity in order to minimise pressure drop and pumping costs. Viscosity plays a major role in determining pumping power requirement of any heat exchanger, thus, precise knowledge of the nanofluids' viscosity behaviour is important [15]. Also, a key problem with nanofluid's research is the estimation of the effective viscosity of nanofluids. Einstein's model [16] showed that the viscosity of colloidal suspensions of spherical particles increases as the volume fraction of suspended particle increases, however the Einstein's model just involve the volume fraction and base fluid viscosity. Brinkman [17], Krieger and Dougherty [18] and Batchelor [19] all modified Einstein's model to show the effect of particle-particle interactions and concentrated volume fraction on the effective viscosity of suspension of solid spheres. However, the effect of size and temperature are not included in the above mentioned models. Therefore, these models have underperformed in most cases when used for predicting the viscosity of nanofluids [20].

Xie et al. [20] discovered that MgO-EG nanofluids formulated from 20 nm MgO have higher thermal conductivity and lower viscosity enhancements than those of ZnO-EG, SiO_2-EG, Al_2O_3-EG and TiO_2-EG all formulated from a similar particle size of their respective nanoparticles. Recently, Hemmat Esfe et al.

[21] investigated the influence of different MgO nanoparticles sizes (20, 40, 50 and 60 nm), temperatures (25-55 ^{o}C) and volume fractions (0.25-5%) on the thermal conductivity of MgO-EG nanofluids and proposed a correlation for predicting the thermal conductivity of the nanofluids. To the best knowledge of the authors there is no study on the viscosity of ethylene glycol based nanofluids containing MgO, which proposes new correlations including particle size, temperature and volume fraction as parameters. In view of this, the viscosity of MgO-EG nanofluids is investigated experimentally considering various particle sizes, volume fractions and temperatures. The measured data are compared with the predictions of different prominent models existing in the literature which show no agreement. Therefore, an empirical-based correlation is developed using the method of dimensional analysis. Furthermore, fuzzy C-means clustering-based adaptive neuro-fuzzy inference system (FCM-ANFIS) and genetic algorithm-polynomial neural network (GA-PNN) modelling techniques [22] are applied for modelling and predicting the effective viscosity of MgO-EG nanofluids as a function of nanoparticle diameter, temperature and nanoparticle volume fraction.

2. Experimental

The two-step method was employed to prepare the MgO-EG nanofluid samples used in the present work. The nanoparticles APS is ~21, ~105 and ~125 nm, to be represented as MgO-I, MgO-II and MgO-III respectively. The transmission electron microscopy (TEM) image and particle size distribution (PSD) of the MgO nanoparticles are as shown in Fig. 1. Presented in Fig. 2 is the X-ray diffraction (XRD) and energy-dispersive spectroscopy (EDS) characterisations for the three nanoparticle samples. The EG used, was procured from Merck Millipore and has 99.5% purity, and viscosity of 16.9 mPa.s at 25 ^{o}C. No surfactant or pH modifier was added in the samples used for viscosity investigations since they were all stable.

To achieve good dispersions in the present study, the required optimum energy density (to form homogeneous nanofluids) was investigated by using Hielscher UP200S ultrasonicator. The energy densities of 2.183×10^{6} kJ/m^{3} to 13.092×10^{6} kJ/m^{3} were applied to the samples and the nanofluids consistency were monitored by viscosity measurements. This is a well-known procedure, to use rheology to characterise the state of dispersion of nanostructures in base fluids [14]. Programmable constant temperature thermal bath (LAUDA ECO RE1225) was used to vary the temperature of the samples within the experimental range (20 to 70 ^{o}C). The viscosity of the samples was measured with a vibro-viscometer (SV-10, A&D, Japan) with 5.0% uncertainty at full range. The viscometer was calibrated using pure EG at 25 ^{o}C and benchmark test were carried out between 20-70 ^{o}C. The result of the benchmark test as presented in Fig. 3 shows good agreement with values reported by Xie et al. [20] and Pastoriza-Gallego et al. [23] within the present experimental uncertainty. A more detailed step-by-step experimental procedure can be found in Adio et al. [24].

The dispersion process and the stability of nanofluid were also characterised by UV-visible spectrophotometer (Model 7315 from Jenway) and zeta potential measurement using Zetasizer Nano ZS (Malvern Instrument Inc., London, UK). The UV-visible analysis is one of the convenient ways to

characterise the dispersion of nanofluid. Using the Beer Lambert law (Eq. 1), the light absorbency ratio index of the nanofluid can be calculated.

$$A_b = -\log \frac{I_o}{I} = \varepsilon l c \quad (1)$$

In Eq. (1), A_b is the absorbance, I_o is the intensity of the UV-visible light through the blank, I is the intensity of the UV-visible light through the samples, ε is the molar absorptivity, l is the length of the light passes through the solution (optical path) and c is the molar concentration of the particles in suspension. The equation shows that for a fix optical path and molar absorptivity, the absorbency of a suspension is proportional to the concentration of the particles present in the suspension. Therefore, a good dispersion will follow the Beer's law [25]. In the UV-visible investigation, volume fraction up to 0.025% was used as higher volume fraction does not allow both UV and visible light to penetrate the sample. Regarding the zeta potential, the equipment (Zetasizer Nano ZS) measures the electrophoretic mobility of the particles using capillary cells with electrodes at either end to which electric potential is applied. The measured electrophoretic mobility of the particle is then used to calculate the zeta potential using the Henry's function. The zeta potential was measured at room temperature (25 ^{o}C) with applied voltage of 10 V. Due to equipment limitation a dilute concentration of 0.05% was used for measurements as higher concentrations were beyond the equipment's range.

3. Results and discussion

The experimental results of the characterisation, and the influence of ultrasonication energy, temperature, volume fraction and particle size on the viscosity of the prepared nanofluids are presented below. Subsequently, the results of modelling with dimensional analysis, FCM-ANFIS and GA-PNN techniques are offered, including comparison with the available viscosity models from the literature.

3.1. Nanofluids characterisation

Fig 4 shows the UV-visible spectra for the nanofluid at different particle concentrations. The spectra patterns show maximum absorption at about 260 nm. As seen in Fig. 4 (a, b and c), the spectra patterns are similar but the absorbance value at a given wavelength increases with increase of MgO nanoparticle concentration. The plots between absorbance and MgO concentration at 260 nm as presented in Fig. 4 (d, e and f) show that the absorbance depends linearly on the MgO nanoparticle concentration and the data obeyed the Beer's law. A zeta potential value of (±30 mV) is the acceptable threshold value for a stable suspension [26]. Therefore, nanofluid sample with zeta potential value (absolute value) greater than or equal to the threshold is considered stable. The zeta potential of all MgO-EG nanofluid samples in the present experiments were above the threshold without modifying their pH values. Here, zeta potential values of 38.5, 46.5 and 30.3 mV were recorded for MgO-I, MgO-II and MgO-III respectively. For the sake of studying the influence of change in pH on zeta potential, the pH of the sample was adjusted using 0.5M KOH and/or HCl before the measurement was made with at least 4 repeated measurements. The average of the repeated measurement was taken as the measured value. Fig. 5 shows the zeta potential

behaviour of nanofluid at different pH. The inset was taken 5 days after preparation and it can be seen that the samples used in this experiment are stable as there was little or no sedimentation even without pH modification or surfactant addition.

3.2. Influence of ultrasonication energy density

Due to the large surface area of nanoparticles, aggregation of nanoparticles often occurs especially when the nanofluid is prepared using the two-step method. The application of ultrasonic vibration during this preparation method have been confirmed to enhance proper homogenisation of the nanoparticles in liquid given that the bonding interaction between the particles that form the aggregates are not always strong [27]. Proper dispersion is very essential to achieving a satisfactory stability and reduced viscosity in the nanofluids. Applying proper ultrasonication to the dispersion process have been shown to reduce the size of aggregates that are usually formed, increase the thermal conductivity and reduce the viscosity of nanofluids [28–30]. Presented in Fig. 6 are the plots of the effective viscosity against the energy density applied for the preparation of the MgO-EG nanofluids for 1% and 3% MgO volume fractions. The results show that at 4.364×10^6 kJ/m^3 energy density, the nanofluid samples are all uniformly dispersed (corresponding to 60 min ultrasonication time, with 80% pulse-to-pulse, 75% amplitude settings on the ultrasonic vibrator for 85 ml samples). Similar trends were obtained for other volume fractions except volume fractions 0.1% and 0.5% that were uniformly homogenised at an energy density of 2.183×10^6 kJ/m^3 which is due to the smaller volume fraction of the nanoparticles. Xie et al. [20] applied ultrasonication for three hours to disperse 20 nm MgO in EG for volume fraction up to 5% Comparing their results with the results obtained on MgO-I (21 nm in size) in the present investigation gave good agreement as shown in Fig. 7. While the energy density applied in their experiment was not mentioned and no data were provided for possible recalculation of their energy input, they applied ultrasonication three times of the period of the present experimental work. Therefore, selecting a predefined value of time for nanofluids preparation, especially in two-step method is counterproductive. Further to the above results, other results presented below are therefore based on the uniformly homogenised nanofluids.

3.3. Influence of temperature on effective viscosity

The effective viscosity of the MgO-EG samples decreases exponentially with increasing temperature as presented in Fig. 8 (a)-(c). At all the volume fractions and irrespective of the particle size, the temperature dependence of the effective viscosity of the MgO-EG nanofluid is similar to the dependence exhibited by the base fluid. However, the viscosity of the nanofluid is higher depending on the concentration of MgO contained in the nanofluid. At higher temperatures (50-70^{o}C) the change in effective viscosity from one volume fraction to the other reduces as overlaps of data points were obvious. This is primarily due to the increase in the influence of temperature in weakening of the intermolecular bonding which drastically reduced the shear resistance of the nanofluids. Interestingly, the relative viscosity when plotted against the working temperature for all volume fractions and nanoparticle sizes

presented nearly a flat line, indicating not much change in relative viscosity with temperature as shown in Fig. 8 (d)-(f).

3.4. Influence of volume fraction and size of MgO nanoparticles

The dispersion of MgO nanoparticles into the base fluid shows that the viscosity of the resulting fluid is higher than that of the ordinary base fluid as presented in Fig. 9 (a). Trends having similar characteristics have been reported in the past on other types of nanofluid [31,32]. Having nanoparticles suspended in the base fluid leads to shear resistance of the nanoparticles on the base fluid layers, and increasing the volume concentration gives a corresponding increase in the shear resistance which is relative to the viscosity of the nanofluid. Therefore, the higher the volume fraction, the more the viscosity enhancement of the nanofluid. The MgO-I samples displayed the highest effective shear viscosity when compared to MgO-II and MgO-III and this is because the particle size of MgO-I is smaller. At the same volume fraction, smaller particle size translates into higher number density of particles present in the suspension, thereby increasing the effective volume fraction [33]. When nanoparticles are uniformly homogenised with reduced aggregate size, the Brownian theory indicates that smaller nanoparticle will have higher dissipation energy and increased particle-particle interactions due to increased particles random motion (higher velocity compared to bigger particles). This phenomenon will increase the viscosity of nanofluid prepared from the smaller particle size compared to those prepared from big particle size [34]. At higher temperature, the volume fraction and size dependence of the viscosity are not dominant as shown in Fig. 9 (a). When the temperature is 70 ^{o}C the effect of increase in volume fraction and change in particle size appear to have disappeared, which further buttressed the fact that the influence of temperature is dominant (Fig. 9 (a)). Also obvious in the relative viscosity plot of Fig. 9 (b) is the level of harmony in the relative viscosity of MgO-II and MgO-III samples for all the volume fractions. This is basically a function of their nanoparticle sizes. From the size analysis presented in Fig. 1 (d), the size of MgO-II and MgO-III are of the same order of magnitude. In addition, unlike other reported results for some types of nanofluids [35], the relative viscosity of the MgO-EG nanofluid appears to increase linearly with volume fraction increase.

3.5. Theoretical models

The established theoretical models that may be used for predicting the viscosity of nanofluids are very limited. Virtually all of these models were derived considering only the influence of particle concentration in suspension [16–19,36] while neglecting the effect of temperature and particle size. Nanofluids are colloidal suspensions which can be treated as a two-phase fluid of solid-liquid mixture and it may be expected that their thermophysical properties would follow the conventional colloids containing micrometric and millimetric particles. However, the applicability of the prominent classical models (designed for micrometric suspensions) to nanofluids is still uncertain [35]. Presented in Table 1 are some of the prominent classical models that are used for the viscosity of nanofluids.

Heyhat et al. [37] proposed an empirical model (Eq. 2) considering both temperature and volume fraction of nanoparticles for Al_2O_3-water nanofluids. Their model was developed with data obtained from 0.1 to 2% Al_2O_3 volume fraction, particle size of 40 nm and temperature range of 20 to 60 ^oC.

$$\mu_{nf} = \mu_o(T)Exp\left(\frac{5.989\phi}{0.278-\phi}\right) \tag{2}$$

Chandreasekar et al. [8] only considered volume fraction of Al_2O_3 in water nanofluid to derive an empirical correlation that is only valid for predicting the viscosity at room temperature (25 ^oC) and for volume fraction of 0.33 to 5%. Their model was developed based on the mean free path between nanoparticles and it is given as:

$$\mu_{nf} = \mu_o\left(1+A\left(\frac{\phi}{1-\phi}\right)^n\right) \tag{3}$$

In the Eq (3), *A* and *n* is taken as 5200 and 2.8 respectively. Chen et al. [38] also considered only the volume fraction of nanoparticle to propose an empirical correlation (Eq. 4) of the form of Batchelor's model [19]. Corcione [39] on the other hand considered nanoparticles size, particle volume fraction and base fluid properties such as molecular mass and density to derive the empirical correlation of Eq. (5). The recent review of Meyer et al [40] gave a comprehensive coverage of the different viscosity models available for nanofluids and other suspensions alike.

$$\mu_{eff} = \mu_o\left(1+10.6\phi+(10.6\phi)^2\right) \tag{4}$$

$$\mu_{eff} = \mu_o\left(\frac{1}{1-34.87(d_p/d_o)^{-0.3}\phi^{1.03}}\right) \tag{5}$$

where $d_o = 0.1\left(\frac{6\overline{M}}{N_A\pi\rho_o}\right)^{1/3}$ is the base fluid molecular diameter.

3.5.1. Dimensional analysis

In the present study, essential parameters which are nanoparticle size, volume fraction temperature, capping layer thickness, viscosity of the base fluid, the density of base fluid and the density of nanofluid are considered as input parameters These parameters are normalised to produce the following non-dimensional parameters (π's) as presented below:

$$\pi_1 = \frac{\mu_{eff}}{\mu_o} = f\left(\pi_2 = \frac{T}{T_0}, \pi_3 = \phi, \pi_4 = \frac{d_p}{h}, \pi_5 = \frac{\rho_{nf}}{\rho_o}\right) \tag{6}$$

In the Eq. (6) above, *T* is the working temperature, T_0 is the reference temperature taken as 20 ^oC, d_p is the particle diameter, *h* is the thickness of the capping layer (nanolayer) taken as 1 nm [41], ρ_o is the density of base fluid and ρ_{nf} is the density of nanofluid. The densities of the nanofluids were calculated based on the mixture model [42] and correlation matrix was run on 198 data points with each data point containing all the four independent non-dimensional parameters. The result of the correlation matrix

shows that π_3 and π_5 are highly correlated with over 99% correlation index. Preference is given to π_3 over π_5 since it is part of the input parameters that is considered in the present experiment. Therefore, Eq. (6) is reduced to Eq. (7).

$$\frac{\mu_{eff}}{\mu_o} = f\left(\frac{T}{T_0}, \phi, \frac{d_p}{h}\right) \tag{7}$$

Using nonlinear regression modelling, the function *f* in Eq. (7) is expressed as follows:

$$\frac{\mu_{eff}}{\mu_o} = 1 + a_0\phi + a_1\left(\frac{T}{T_0}\right)\phi + a_2\left(\frac{d_p}{h}\right)\phi + a_3\left(\frac{T}{T_0}\right)\phi + a_4\left(\left(\frac{d_p}{h}\right)\phi\right)^2 + a_5\left(\left(\frac{T}{T_0}\right)\phi\right)^2 + a_6\phi^2 + a_7\left(\frac{T}{T_0}\right)^2\phi^{\frac{1}{3}} \tag{8}$$

where $a_0 - a_7$ are empirical constants given as a_0 = 7.0764, a_1 = -1.4334, a_2 = -0.0346, a_3 = 1.3090, a_4 = -0.0024, a_5 = -1.2357, a_6 = 53.6946 and a_7 =0.0436. This correlation is valid for volume fraction of MgO ≤ 5%, temperature between 20-70 ^{o}C and particle size between 21 and 125 nm. The coefficient of determination (R^2) of this model is 0.9524 and other statistics on the goodness of the fit such as the sum of square error (SSE), means square error (MSE) and root mean square error (RMSE) are 0.1564, 0.0008 and 0.0287 respectively. In Fig. 10 the relative viscosity of the MgO-EG nanofluids predicted by using Eq. (8) is compared with the predictions made by some of the prominent models that are used for nanofluid viscosity. It is obvious that the presented correlation performed better than the other models. The models of Einstein [16], Brinkman [17] and Batchelor [19] all predicted almost similar results, which fell short of the present results. The deviation from the experimental results becomes more pronounced as the nanoparticle size gets smaller. On the other hand the empirical models of Kitano et al. [36] which considered particle volume fraction and agglomeration, and Corcione [39] which considered particle size, base fluid properties and volume fraction, both over predicted the present experimental data. In the prediction made by Corcione [39], it can be seen that for the smaller nanoparticle size the deviation from experimental data is also higher than for samples with bigger nanoparticle size. When the correlation in Eq. (8) was used to estimate the temperature dependence of the effective viscosity of MgO-EG nanofluid containing MgO-I nanoparticle sample, it gave very good agreement (Fig. 11). Similar results were obtained for MgO-II and MgO-III samples.

3.5.2. FCM-ANFIS modelling technique and GA-PNN hybrid system

An efficient approach for modelling various systems can be created through the combination of fuzzy techniques and artificial neural network (ANN). The deficiencies in either of the two methods can be minimised by the other method, thereby increasing the efficiency of the system (neuro-fuzzy). There are numerous arrangements that have been proposed for the establishment of an efficient neuro-fuzzy system, however, the adaptive neuro-fuzzy Inference system (ANFIS) technique [43] is one of the most important techniques wherein integrated learning approaches and learning algorithms coincides. Modelling through the use of ANFIS system uses the combination of both fuzzy logic and neural network to achieve accurate results. The fuzzy logic algorithm computes the best membership functions that allow

the inference system to model the input-output relationship of the data. The membership functions are adjusted (adaptive) based on the structure of the data, using the simulation capability of the neural network. The adaptive nature allows the neuro-fuzzy system to learn from the data that is being modelled. The ANFIS architecture is divided into the introductory part (which consist of the input, input characteristics and input membership functions) and the concluding part (which consist of the output characteristics, output membership functions and output). The introductory and the concluding parts are connected together by rules. ANFIS consists of 5 major layers with each layer comprised of nodes/neurons that are of the same functional family. The first layer is an adaptive layer in which the fuzzy formation takes place. The second layer comprised of fixed nodes and here is where fuzzy rules are performed. In the third layer the nodes are fixed and the output of this layer is normalised membership functions. The fourth layer is made up of adaptive nodes, which perform the concluding part of the fuzzy rules and in the fifth layer is a fixed single node that computes the overall network output. A more detailed information on ANFIS network architecture can be found in Mehrabi et al. [44,45]. ANFIS structure can be generated using either of the following structure identification techniques; fuzzy C-mean clustering, subtractive clustering and grid partitioning. Each of these identification techniques follows the steps of mapping the input variables to the input space partitioning, then choosing the appropriate input membership functions, followed by the creation of the fuzzy rules, selection premise and creation of the concluding part of the fuzzy rules and lastly selection of the initial parameters for the membership functions.

Regarding the GA-PNN hybrid system which has also been applied for modelling of the effective viscosity for MgO-EG nanofluid in the present work. The GA-PNN hybrid system was created by a combination of genetic algorithm and the group method of data handling (GMDH)-type polynomial neural network (PNN) approaches. This hybrid system instructs the PNN network using GMDH learning algorithm. In the GA-PNN hybrid system, the GMDH learning algorithm applied to the PNN network introduced the GMDH-PNN for the eventual GA-PNN hybrid system. On the other hand, the hidden layers and the appropriate bias coefficient of the GMDH-PNN (which are necessary for achieving optimal structure and minimising training error) are generated by GA algorithm. Further information regarding GMDH-PNN architecture and GA-PNN hybrid system is given in Pesteei and Mehrabi [46] and Mehrabi et al. [22,47] respectively.

The present experimental data consisting of 198 input-output data points are used in order to predict the effective viscosity for MgO-EG nanofluid. The experimental data were divided into two, with 154 data points (78%) for training and 44 data points (22%) for testing purposes. The root mean square errors (*RMSE*), mean relative error (*MRE*) and mean absolute error (*MAE*) as given in Eqs. (9) to (11) are used as statistical criteria for selecting the optimal model. These criteria show the accuracy of the models used for the prediction of the effective viscosity of MgO-EG nanofluid for various values of input variables.

$$MAE = \frac{1}{n}\sum_{i=1}^{n}\left|X_{pr} - X_{a}\right| \tag{9}$$

$$MRE(\%) = \frac{100}{n}\sum_{i=1}^{n}\left(\frac{\left|X_{pr} - X_a\right|}{X_a}\right) \tag{10}$$

$$RMSE = \sqrt{\frac{1}{n}\sum_{i=1}^{n}\left(X_{pr} - X_a\right)^2} \tag{11}$$

where X_{pr}, is the predicted value, X_a is the experimental value and n is the number of data points. The network architecture of the GA-PNN model for predicting the effective viscosity of MgO-EG nanofluid is shown in Fig. 12, and corresponds to the genome representation of ***3333111222223313,*** in which ***1, 2*** and ***3*** stand for average particle diameter d_p (nm), volume concentration ϕ (%) and Temperature T (^{o}C) respectively. The equivalent grand polynomial model for the effective viscosity of MgO-EG nanofluid based on the network architecture is presented in Appendix A.

Fig. 13 (a) shows the comparison between the present experimental results, FCM-ANFIS model, GA-PNN model and the present correlation presented in (Eq.8) for the viscosity of MgO-EG nanofluid with MgO-I sample at 1% volume fraction and various temperatures between 20 and 70 ^{o}C. All the models for the effective viscosity of MgO-EG nanofluid agree with the experimental data and they present very good degrees of accuracy. The following statistics on the goodness of the predictions were obtained: *RMSE* = 0.095, *MRE* = 0.87% and *MAE* = 0.073 for the correlation (Eq. 8); *RMSE* = 0.529, *MRE* = 2.67% and *MAE* = 0.359 for the GA-PNN model; and *RMSE* = 0.207, *MRE* = 1.32% and *MAE* = 0.148 for FCM-ANFIS model. In Figs. 13 (b)–(d) similar comparisons are made between the results of the three modelling techniques presented in this paper and the experimental results of MgO-II and MgO-III samples respectively. It can be seen that for the temperature regime and the different volume fractions the three models performed very well. Fig. 13 (b and c) contains experimental data for MgO-II sample at 0.5% and 2% volume fractions respectively while Fig. 13 (d) contains experimental data for MgO-III sample at 3% volume fraction. The statistics on the goodness of these fits are very similar to those presented for Fig. 13 (a).

4. Conclusion

MgO nanoparticles of varying sizes between 21 to 125 nm have been dispersed in EG base fluid and were uniformly homogenised using ultrasonication method. The dispersion and stability of the nanofluid samples were characterised using UV-visible spectrophotometry and zeta potential measurement, respectively. Temperature, volume fraction and particle size dependence of the viscosity of the MgO-EG nanofluids were investigated. The values obtained from some of the prominent classical and empirical models were different from the present experimental data Therefore, new viscosity correlations were developed using dimensional analysis, GA-PNN and FCM-ANFIS modelling techniques. The following conclusions are obtained from the study:

i. The absorbance of the nanofluid followed the Beer's Law, showing that the preparation method gave good dispersion. Also, the nanofluid samples are stable without pH

modification as the zeta potential values surpass the stability threshold and there was no sign of sedimentation days after the preparation.

ii. The viscosity of both the base fluid and the nanofluids reduced exponentially with increasing temperature. Also, as particle size increases, the effective viscosity of the nanofluid reduced.

iii. The viscosity of the MgO-EG nanofluids increased linearly with increasing volume fraction. This trend was observed for all the particle sizes investigated.

iv. The prominent theoretical and empirical models were unable to predict the viscosity of the MgO-EG nanofluids. Consequently, correlations based on dimensional analysis, GA-PNN and FCM-ANFIS were proposed to estimate the viscosity of the nanofluid based on experimental data.

v. The proposed dimensional analysis correlation (Eq. 8), GA-PNN and FCM-ANFIS models all perform with a good level of agreement with the experimental data.

vi. Lastly, this work showed the capability of artificial intelligence techniques for modelling engineering problems based on the input-output experimental data.

Acknowledgement

The authors gratefully acknowledge the funding obtained from the National Research Foundation of South Africa (NRF), Stellenbosch University/University of Pretoria Solar Hub, CSIR, EEDSM Hub, NAC, RDP and IRT seed.

Appendix A

Grand GA-PNN model:

$$L_{11} = a_{1,0} + a_{1,1}.d_p + a_{1,2}.\phi + a_{1,3}.d_p.\phi + a_{1,4}.{d_p}^2 + a_{1,5}.\phi^2$$

$$L_{21} = a_{2,0} + a_{2,1}.T + a_{2,2}.d_p + a_{2,3}.T.d_p + a_{2,4}.T^2 + a_{2,5}.{d_p}^2$$

$$L_{12} = a_{3,0} + a_{3,1}.d_p + a_{3,2}.L_{11} + a_{3,3}.d_p.L_{11} + a_{3,4}.{d_p}^2 + a_{3,5}.{L_{11}}^2$$

$$L_{22} = a_{4,0} + a_{4,1}.\phi + a_{4,2}.L_{21} + a_{4,3}.\phi.L_{21} + a_{4,4}.\phi^2 + a_{4,5}.{L_{21}}^2$$

$$L_{13} = a_{5,0} + a_{5,1}.T + a_{5,2}.L_{12} + a_{5,3}.T.L_{12} + a_{5,4}.T^2 + a_{5,5}.{L_{12}}^2$$

$$L_{23} = a_{6,0} + a_{6,1}.\phi + a_{6,2}.L_{22} + a_{6,3}.\phi.L_{22} + a_{6,4}.\phi^2 + a_{6,5}.{L_{22}}^2$$

$$EV = a_{7,0} + a_{7,1}.L_{13} + a_{7,2}.L_{23} + a_{7,3}.L_{13}.L_{23} + a_{7,4}.{L_{13}}^2 + a_{7,5}.{L_{23}}^2$$

Coefficient matrix:

$$\left[\mathbf{a}_{i,j}\right] = \begin{bmatrix} 13.04471101 & -0.23643914 & -0.07431895 & 0.00173761 & 0.36614326 & -0.01084868 \\ 43.42309576 & -0.02706623 & -1.12543872 & -0.00001994 & 0.00819309 & 0.00044192 \\ 14.36973131 & -0.09765461 & -1.28875574 & 0.00050633 & 0.09269148 & 0.00280595 \\ 13.73583221 & -0.12049393 & -0.48198892 & -0.00026002 & 0.04173937 & 0.00491979 \\ 26.50248649 & -0.77882891 & 1.07065759 & 0.00695986 & 0.00836354 & -0.01844119 \\ -0.14756145 & -0.08250359 & 0.96488446 & 0.00870994 & -0.00369486 & 0.05667468 \\ 0.47357046 & -0.07974226 & 0.96704951 & 0.07986601 & 0.05545359 & -0.13097044 \end{bmatrix}$$

References

[1] D.P.D. Kulkarni, P.P.K. Namburu, H. Ed Bargar, D.K. Das, Convective Heat Transfer and Fluid Dynamic Characteristics of SiO_2 Ethylene Glycol/Water Nanofluid, Heat Transf. Eng. 29 (2008) 1027–1035.

[2] D. Zhu, X. Li, N. Wang, X. Wang, J. Gao, H. Li, Dispersion behavior and thermal conductivity characteristics of Al_2O_3–H_2O nanofluids, Curr. Appl. Phys. 9 (2009) 131–139.

[3] J.A. Eastman, S.U.S. Choi, S. Li, W. Yu, L.J. Thompson, Anomalously increased effective thermal conductivities of ethylene glycol-based nanofluids containing copper nanoparticles, Appl. Phys. Lett. 78 (2001) 718–720.

[4] H.U. Kang, S.H. Kim, J.M. Oh, Estimation of Thermal Conductivity of Nanofluid Using Experimental Effective Particle Volume, Exp. Heat Transf. 19 (2006) 181–191.

[5] S.M.S. Murshed, K.C. Leong, C. Yang, Enhanced thermal conductivity of TiO_2 - Water based nanofluids, Int. J. Therm. Sci. 44 (2005) 367–373.

[6] S.K. Das, N. Putra, P. Thiesen, W. Roetzel, Temperature Dependence of Thermal Conductivity Enhancement for Nanofluids, J. Heat Transfer. 125 (2003) 567–574.

[7] S.M.S. Murshed, K.C. Leong, C. Yang, Investigations of thermal conductivity and viscosity of nanofluids, Int. J. Therm. Sci. 47 (2008) 560–568.

[8] M. Chandrasekar, S. Suresh, A.C. Bose, Experimental investigations and theoretical determination of thermal conductivity and viscosity of Al_2O_3/water nanofluid, Exp. Therm. Fluid Sci. 34 (2010) 210–216.

[9] L. Fedele, L. Colla, S. Bobbo, Viscosity and thermal conductivity measurements of water-based nanofluids containing titanium oxide nanoparticles, Int. J. Refrig. 35 (2012) 1359–1366.

[10] E. V Timofeeva, D.S. Smith, W. Yu, D.M. France, D. Singh, J.L. Routbort, Particle size and interfacial effects on thermo-physical and heat transfer characteristics of water-based alpha-SiC nanofluids., Nanotechnology. 21 (2010) 1–10.

[11] J. Zhao, Z. Luo, M. Ni, K. Cen, Dependence of nanofluid viscosity on particle size and pH value, Chin. Phys. Lett. 26 (2009) 1–3.

[12] X.F. Li, D.S. Zhu, X.J. Wang, N. Wang, J.W. Gao, H. Li, Thermal conductivity enhancement dependent pH and chemical surfactant for Cu-H_2O nanofluids, Thermochim. Acta. 469 (2008) 98–103.

[13] Y. Yang, E.A. Grulke, Z.G. Zhang, G. Wu, Thermal and rheological properties of carbon nanotube-in-oil dispersions, J. Appl. Phys. 99 (2006) 114307–1 –8.

[14] Y.S. Song, J.R. Youn, Influence of dispersion states of carbon nanotubes on physical properties of epoxy nanocomposites, Carbon N. Y. 43 (2005) 1378–1385.

[15] M. Mehrabi, M. Sharifpur, J.P. Meyer, Viscosity of nanofluids based on an artificial intelligence model, Int. Commun. Heat Mass Transf. 43 (2013) 6–11.

[16] A. Einstein, A New Determination of Molecular Dimensions, Ann. Phys. 4 (1906) 37–62.

[17] H.C. Brinkman, The viscosity of concentrated suspensions and solutions, J. Chem. Phys. 20 (1952) 571.

[18] I. Krieger, T. Dougherty, A mechanicsm for non-Newtonian flow in suspensions of rigid spheres, Trans. Soc. Rheol. 3 (1959) 137–152.

[19] G. Batchelor, The effect of Brownian motion on the bulk stress in the suspension of sphrerical particles, J. Fluid Mech. 83 (1977) 97–117.

[20] H. Xie, W. Yu, W. Chen, MgO nanofluids: higher thermal conductivity and lower viscosity among ethylene glycol-based nanofluids containing oxide nanoparticles, J. Exp. Nanosci. 5 (2010) 463–472.

[21] M.H. Esfe, S. Saedodin, M. Bahiraei, D. Toghraie, O. Mahian, S. Wongwises, Thermal conductivity modeling of MgO/EG nanofluids using experimental data and artificial neural network, J. Therm. Anal. Calorim. 118 (2014) 287–294.

[22] M. Mehrabi, M. Sharifpur, J.P. Meyer, Application of the FCM-based neuro-fuzzy inference system and genetic algorithm-polynomial neural network approaches to modelling the thermal conductivity of alumina--water nanofluids, Int. Commun. Heat Mass Transf. 39 (2012) 971–997.

[23] M.J. Pastoriza-Gallego, L. Lugo, J.L. Legido, M.M. Piñeiro, Thermal conductivity and viscosity measurements of ethylene glycol-based Al_2O_3 nanofluids., Nanoscale Res. Lett. 6 (2011) 221–231.

[24] S.A. Adio, M. Sharifpur, J.P. Meyer, Investigation Into Effective Viscosity, Electrical Conductivity, and pH of γ- Al_2O_3-Glycerol Nanofluids in Einstein Concentration Regime, Heat Transf. Eng. 36 (2015) 1241–1251.

[25] M. Mehrali, E. Sadeghinezhad, S.T. Latibari, S.N. Kazi, M. Mehrali, M.N.B.M. Zubir, et al., Investigation of thermal conductivity and rheological properties of nanofluids containing graphene nanoplatelets., Nanoscale Res. Lett. 9 (2014) 1–12.

[26] R. Greenwood, Review of the measurement of zeta potentials in concentrated aqueous suspensions using electroacoustics, Adv. Colloid Interface Sci. 106 (2003) 55–81.

[27] S.J.J. Chung, J.P.P. Leonard, I. Nettleship, J.K.K. Lee, Y. Soong, D.V. V Martello, et al., Characterization of ZnO nanoparticle suspension in water: Effectiveness of ultrasonic dispersion, Powder Technol. 194 (2009) 75–80.

[28] K. Suganthi, N. Anusha, K. Rajan, Low viscous ZnO–propylene glycol nanofluid: a potential coolant candidate, J. Nanoparticle Res. 15 (2013) 1986–1–6.

[29] S.A. Adio, M. Sharifpur, J.P. Meyer, Influence of ultrasonication energy on the dispersion consistency of Al_2O_3–glycerol nanofluid based on viscosity data, and model development for the required ultrasonication energy density, J. Exp. Nanosci. (2015). doi:10.1080/17458080.2015.1107194.

[30] M. Sharifpur, S.A. Adio, J.P. Meyer, Experimental investigation and model development for effective viscosity of Al_2O_3–glycerol nanofluids by using dimensional analysis and GMDH-NN methods, Int. Commun. Heat Mass Transf. 68 (2015) 208–219.

[31] M. Ghazvini, M.A. Akhavan-Behabadi, E. Rasouli, M. Raisee, Heat Transfer Properties of Nanodiamond–Engine Oil Nanofluid in Laminar Flow, Heat Transf. Eng. 33 (2012) 525–532.

[32] N. Singh, G. Chand, S. Kanagaraj, G. Ghand, Investigation of Thermal Conductivity and Viscosity of Carbon Nanotubes–Ethylene Glycol Nanofluids, Heat Transf. Eng. 33 (2012) 821–827.

[33] B.A. Horri, P. Ranganathan, C. Selomulya, H. Wang, A new empirical viscosity model for ceramic suspensions, Chem. Eng. Sci. 66 (2011) 2798–2806.

[34] Z. Jia-Fei, L. Zhong-Yang, Dependence of nanofluid viscosity on particle size and pH value, Chinese Phys. Lett. 26 (2009) 10–13.

[35] M. Kole, T.K. Dey, Viscosity of alumina nanoparticles dispersed in car engine coolant, Exp. Therm. Fluid Sci. 34 (2010) 677–683.

[36] T. Kitano, T. Kataoka, T. Shirota, An empirical equation of the relative viscosity of polymer melts filled with various inorganic fillers, Rheol. Acta. 20 (1981) 207–209..

[37] M.M.M. Heyhat, F. Kowsary, A.M.M. Rashidi, M.H. Memenpour, A. Amrollahi, M.H. Momenpour, Exeprimental investigation of laminar convective heat transfer and pressure drop of water-based Al_2O_3 nanofluids in fuly developed flow regime, Exp. Therm. Fluid Sci. 44 (2013) 483–489.

[38] H. Chen, Y. Ding, Y. He, C. Tan, Rheological behaviour of ethylene glycol based titania nanofluids, Chem. Phys. Lett. 444 (2007) 333–337.

[39] M. Corcione, Empirical correlating equations for predicting the effective thtermal conductivity and dynamic viscosity of nanofluids, Energy Convers. Manag. 52 (2011) 789–793.

[40] J.P. Meyer, S.A. Adio, M. Sharifpur, P.N. Nwosu, The viscosity of nanofluids: a review of the theoretical, empirical and numerical models, Heat Transf. Eng. 37 (2016) 387–421.

[41] S. Hosseini, A. Moghadassi, D.E. Henneke, A new dimensionless group model for determining the viscosity of nanofluids, J. Therm Anal Calorim. 100 (2010) 873–877.

[42] K. Khanafer, K. Vafai, A critical synthesis of thermophysical characteristics of nanofluids, Int. J. Heat Mass Transf. 54 (2011) 4410–4428.

[43] J.S.R. Jang, ANFIS: adaptive-network-based fuzzy inference system, IEEE Trans. Syst. Man Cybern. 23 (1993) 665–685.

[44] M. Mehrabi, S.M. Pesteei, T. Pashaee G., Modeling of heat transfer and fluid flow characteristics of helicoidal double-pipe heat exchangers using Adaptive Neuro-Fuzzy Inference System (ANFIS), Int. Commun. Heat Mass Transf. 38 (2011) 525–532.

[45] M. Mehrabi, M. Sharifpur, J.P. Meyer, Adaptive Neuro-Fuzzy Modeling of the Thermal Conductivity of Alumina-Water Nanofluids, in: ASME 2012 Third Int. Conf. Micro/Nanoscale Heat Mass Transf., ASME, Atlanta, GA, 2012: pp. 155–161.

[46] S.M. Pesteei, M. Mehrabi, Modeling of convection heat transfer of supercritical carbon dioxide in a vertical tube at low Reynolds numbers using artificial neural network, Int. Commun. Heat Mass Transf. 37 (2010) 901–906.

[47] M. Mehrabi, S. Rezazadeh, M. Sharifpur, J.P. Meyer, Modeling of Proton Exchange Membrane Fuel Cell (PEMFC) Performance by Using Genetic Algorithm-Polynomial Neural Network (GA-PNN) Hybrid System, in: ASME 2012 10th Int. Conf. Fuel Cell Sci. Eng. Technol., ASME, San Diego, CA, 2012: pp. 447–452.

Table 1 Summarised list of the available classical models

Investigator	Classical Model	Remark
Einstein [16]	$\mu_{eff} = \mu_o (1 + 2.5\phi)$	Established on extremely dilute suspension of rigid solid spheres and non-interacting medium. Volume fraction of $\phi \leq 0.02$. From the model, it is clear that viscosity is a linear function of volume fraction.
Brinkman [17]	$\mu_{eff} = \mu_o (1 - \phi)^{-2.5}$	This is an extension of [16] and for a volume fraction, $\phi \leq 0.04$.
Krieger and Dougherty [18]	$\mu_{eff} = \mu_o \left(1 - \frac{\phi}{\phi_m}\right)^{-[\eta]\phi_m}$	Covers virtually the whole spectrum of nanoparticles. ϕ_m is the maximum concentration at which flow can occur, and its value for high shear rate is 0.605. η is the intrinsic viscosity with a typical value of 2.5.
Batchelor [19]	$\mu_{eff} = \mu_o (1 + 2.5\phi + 6.5\phi^2)$	Effect of interactions between particles was considered in the development of this model. Within the limits of a very low particle volume concentration, this model approaches model [16].

Figure Caption

Fig.1. TEM image of MgO and particle size distribution (a) MgO- I (b) MgO-II (c) MgO-III (d) particles size distribution.

Fig. 2. XRD and EDS spectral patterns of MgO nanoparticles (a) XRD spectral of MgO-I, MgO-II and MgO-III respectively, (b, c and d) EDS spectral of MgO-III, MgO-II and MgO-I respectively.

Fig. 3. Plot of the benchmark tests with the base fluid (EG) and comparison with experimental data from the literature.

Fig. 4 UV-visible of MgO-EG nanofluid at different concentation (a)-(c) UV-visible spectra between 230-900 nm (d)-(f) relationships between the absorbance and concentration of the nanofluid at 260 nm.

Fig. 5 Influence of change in pH on the zeta potential of MgO-EG nanofluid.

Fig. 6. Effect of energy density on the viscosity of MgO-EG nanofluid (a) 1% volume fraction (b) 3% volume fraction.

Fig. 7. Comparison between the present MgO-I experimental data literature data of Xie et al. [20]. (a) 1% volume fraction (b) 3% volume fraction.

Fig. 8. Effect of temperature on the effective viscosity and relative viscosity at various volume fractions (a)-(c) effective viscosity vs. temperature for MgO-I, MgO-II and MgO-III respectively, and (d)-(f) relative viscosity vs. temperature for MgO-I, MgO-II and MgO-III respectively.

Fig.9. Viscosity against volume fraction (a) effective viscosity at 20 and 70 ^{o}C (b) normalised effective viscosity.

Fig 10. Comparison between the present experimental data, proposed correlation (Eq. 8) and other prominent viscosity models.

Fig. 11 Comparison between experimental data (effective viscosity of MgO-EG) and the proposed correlation (Eq.8) for different temperatures and various volume fractions, in the case of 21 nm particles size.

Fig. 12 Structure of the GA-PNN hybrid system for the effective viscosity of MgO-EG nanofluid modelling.

Fig. 13 Comparison of the experimental data with the GA-PNN model, FCM-ANFIS model and proposed model for the effective viscosity of MgO-EG nanofluid (a) MgO-I at 1% volume fraction (b) MgO-II sample at 0.5% volume fraction (c) MgO-II at 2% volume fraction and (d) MgO-III at 3% volume fraction.

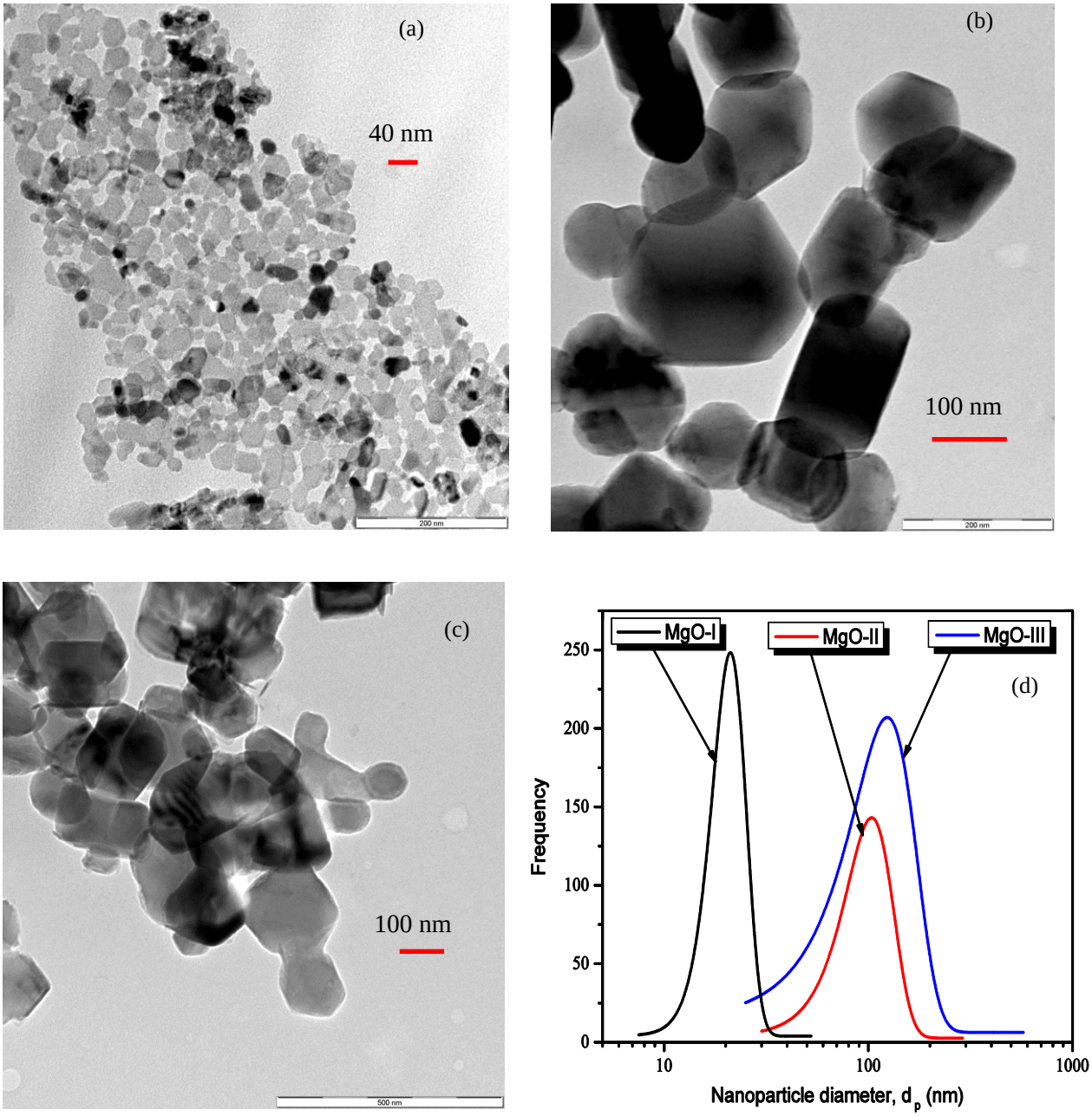
(a)
40 nm
(b)
100 nm
(c)
100 nm
(d)
MgO-I
MgO-II
MgO-III
Frequency
Nanoparticle diameter, d p (nm)
0
50
100
150
200
250
10
100
1000

Fig.1.

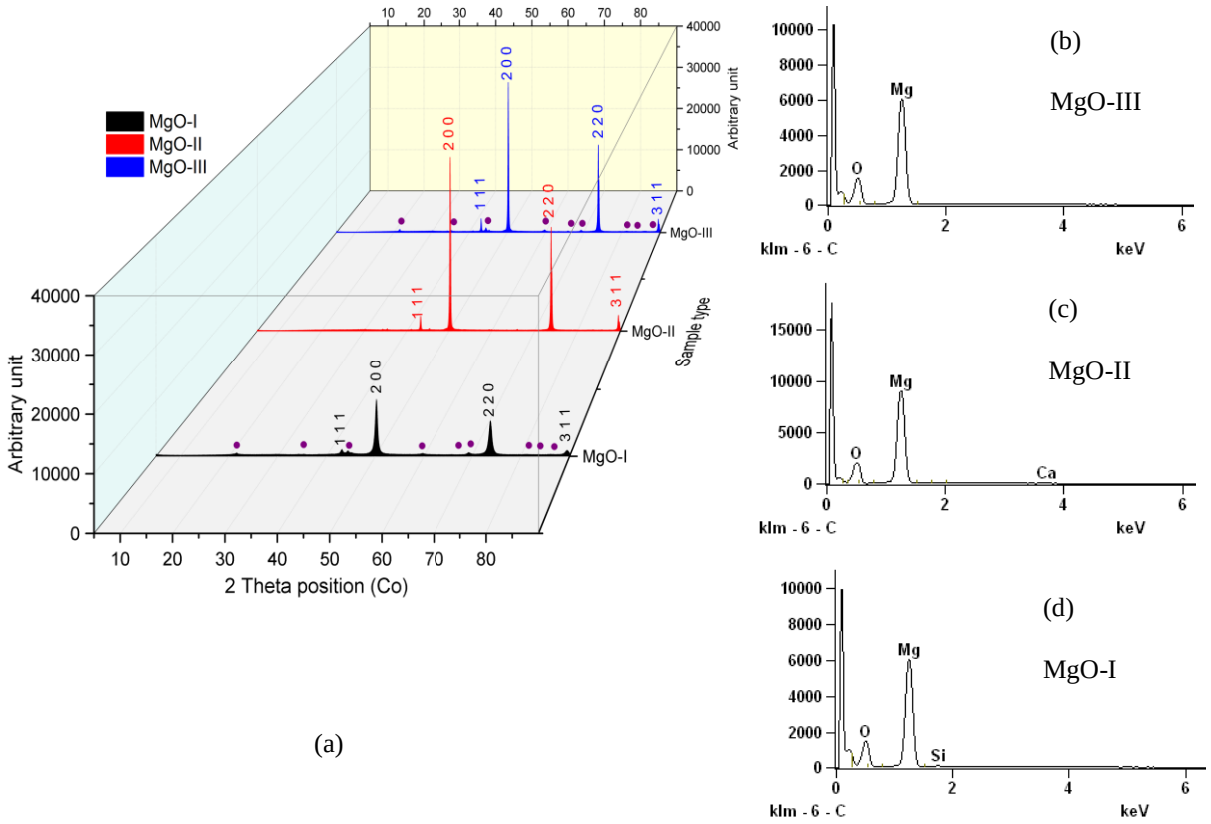
MgO-I
MgO-II
MgO-III
Arbitrary unit
2 Theta position (Co)
Sample type
(a)
(b)
MgO-III
(c)
MgO-II
(d)
MgO-I
Mg
O
Ca
Si
klm - 6 - C
keV

Fig. 2.

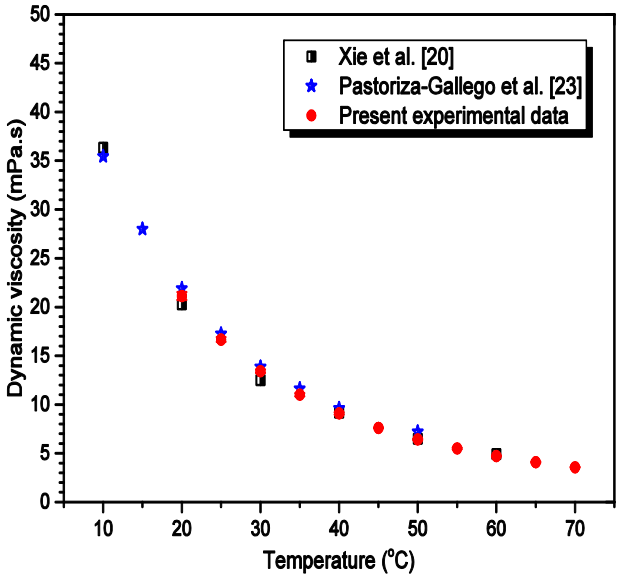
Xie et al. [20]
Pastoriza-Gallego et al. [23]
Present experimental data
Dynamic viscosity (mPa.s)
Temperature (°C)
0
5
10
15
20
25
30
35
40
45
50
10
20
30
40
50
60
70

Fig. 3

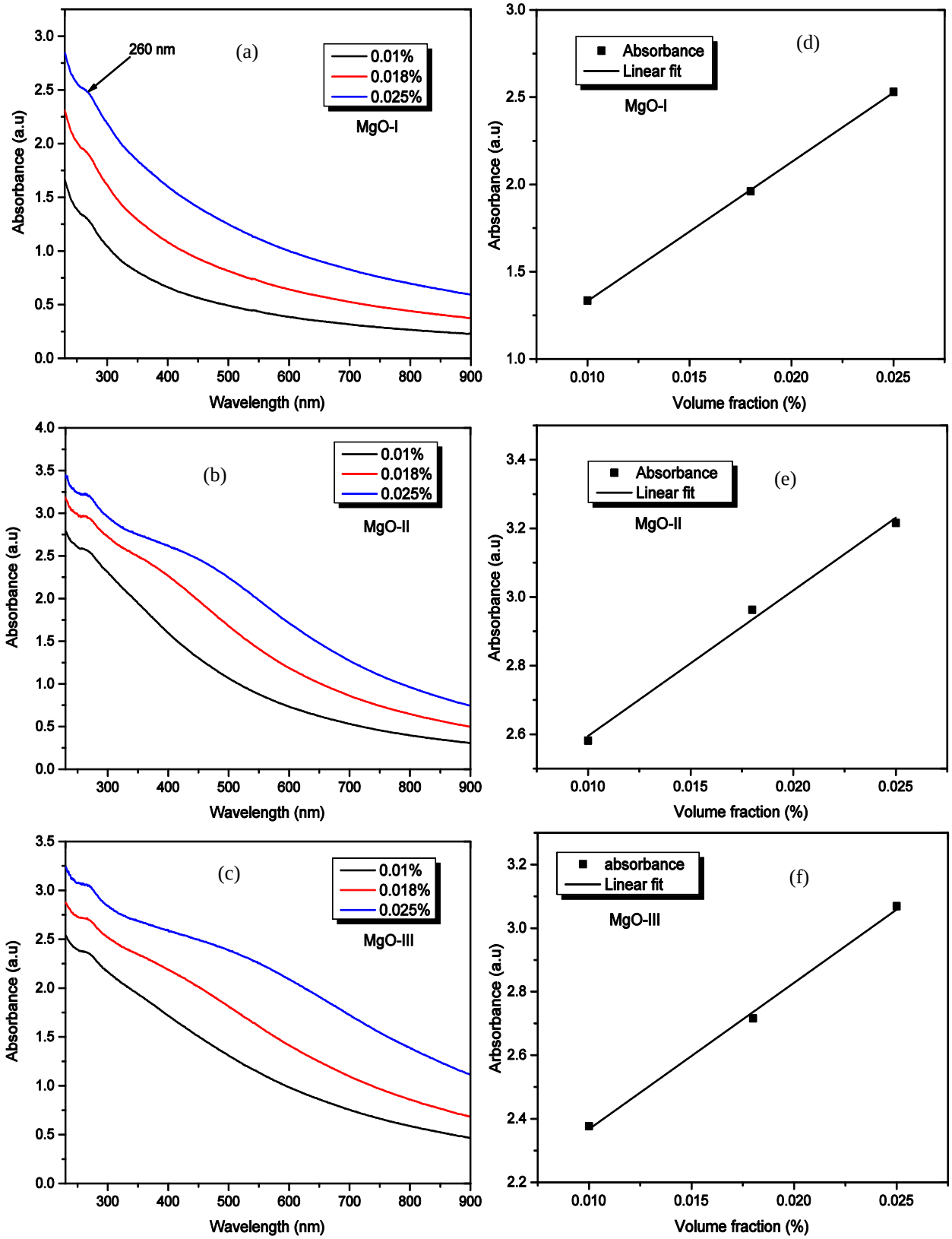
(a)
260 nm
0.01%
0.018%
0.025%
MgO-I
Absorbance (a.u)
Wavelength (nm)
(d)
Absorbance
Linear fit
MgO-I
Arbsorbance (a.u)
Volume fraction (%)
(b)
0.01%
0.018%
0.025%
MgO-II
Absorbance (a.u)
Wavelength (nm)
(e)
Absorbance
Linear fit
MgO-II
Arbsorbance (a.u)
Volume fraction (%)
(c)
0.01%
0.018%
0.025%
MgO-III
Absorbance (a.u)
Wavelength (nm)
(f)
absorbance
Linear fit
MgO-III
Arbsorbance (a.u)
Volume fraction (%)

Fig. 4

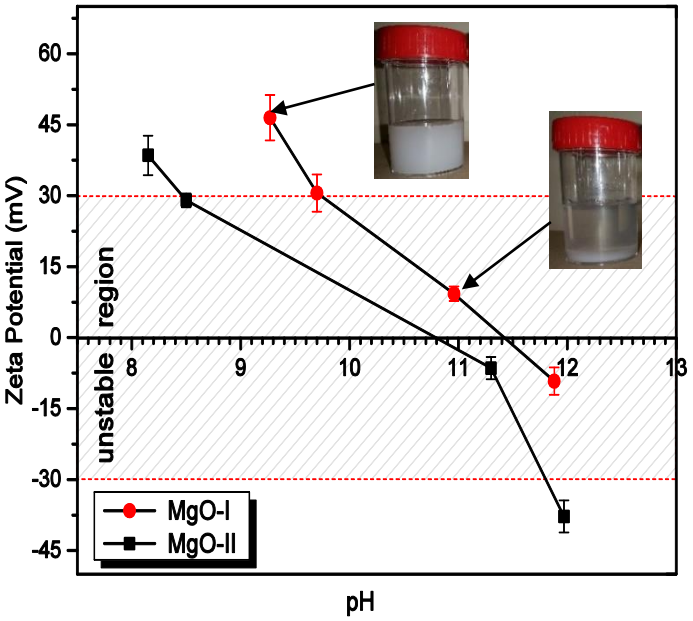
Zeta Potential (mV)
60
45
30
15
0
-15
-30
-45
unstable region
8
9
10
11
12
13
pH
MgO-I
MgO-II

Fig. 5

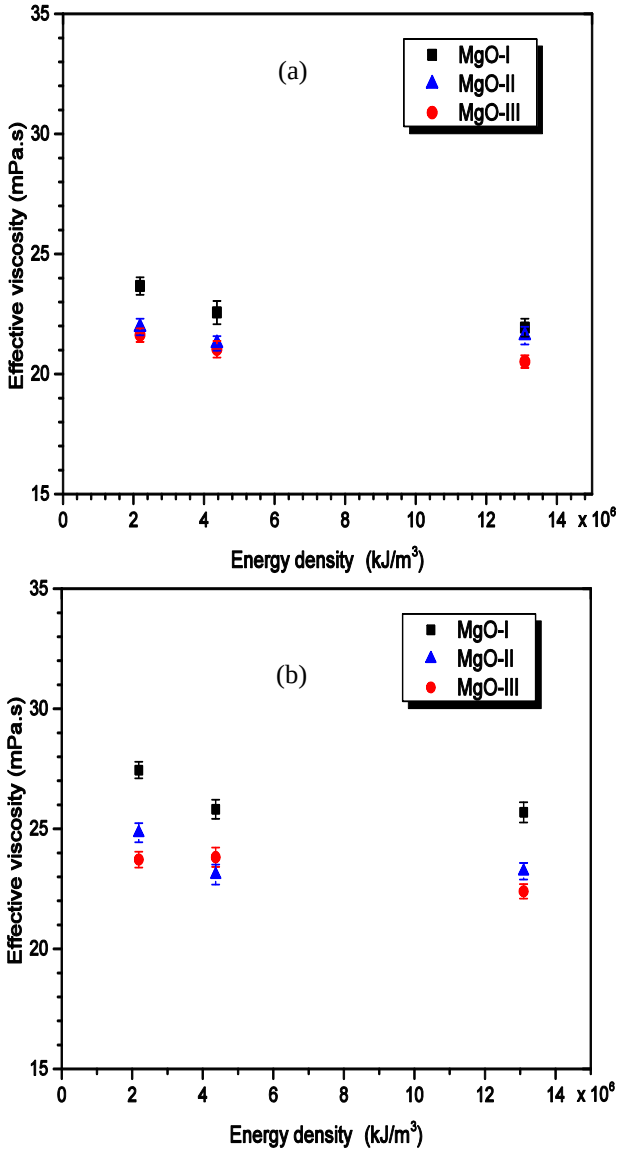
(a)
MgO-I
MgO-II
MgO-III
Effective viscosity (mPa.s)
Energy density (kJ/m3)
x 10^6
(b)
MgO-I
MgO-II
MgO-III
Effective viscosity (mPa.s)
Energy density (kJ/m3)
x 10^6

Fig. 6.

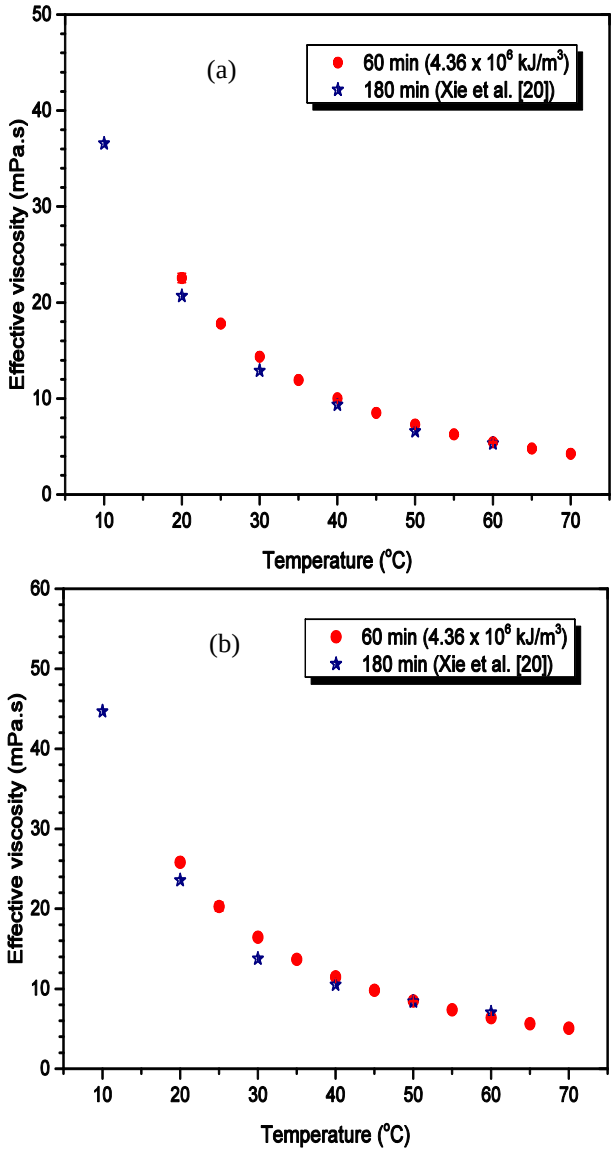
(a)
60 min (4.36 x 10^6 kJ/m^3)
180 min (Xie et al. [20])
Effective viscosity (mPa.s)
Temperature (°C)
(b)
60 min (4.36 x 10^6 kJ/m^3)
180 min (Xie et al. [20])
Effective viscosity (mPa.s)
Temperature (°C)

Fig. 7.

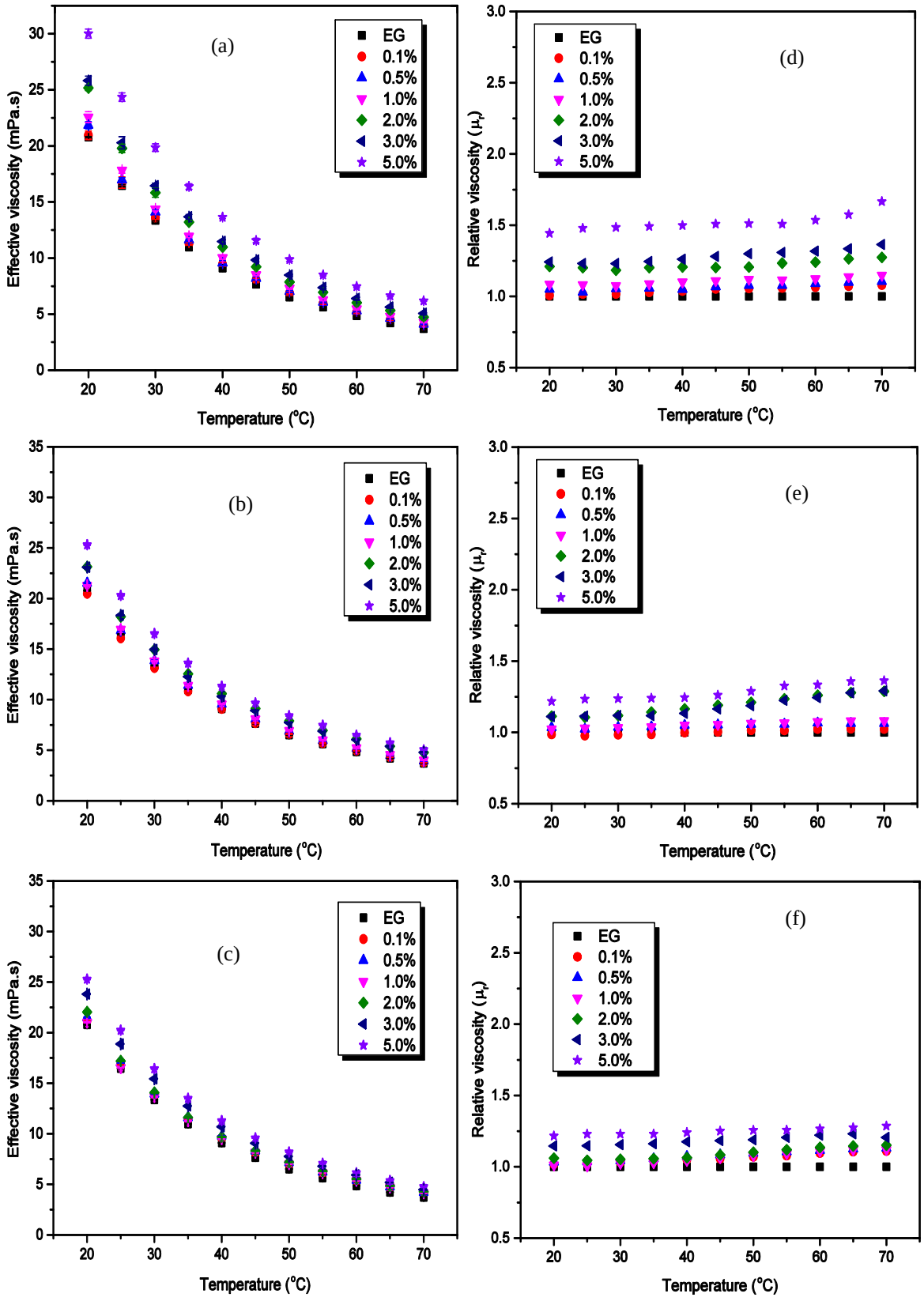
(a)
(b)
(c)
(d)
(e)
(f)
EG
0.1%
0.5%
1.0%
2.0%
3.0%
5.0%
Effective viscosity (mPa.s)
Relative viscosity (μ_r)
Temperature (°C)

Fig 8

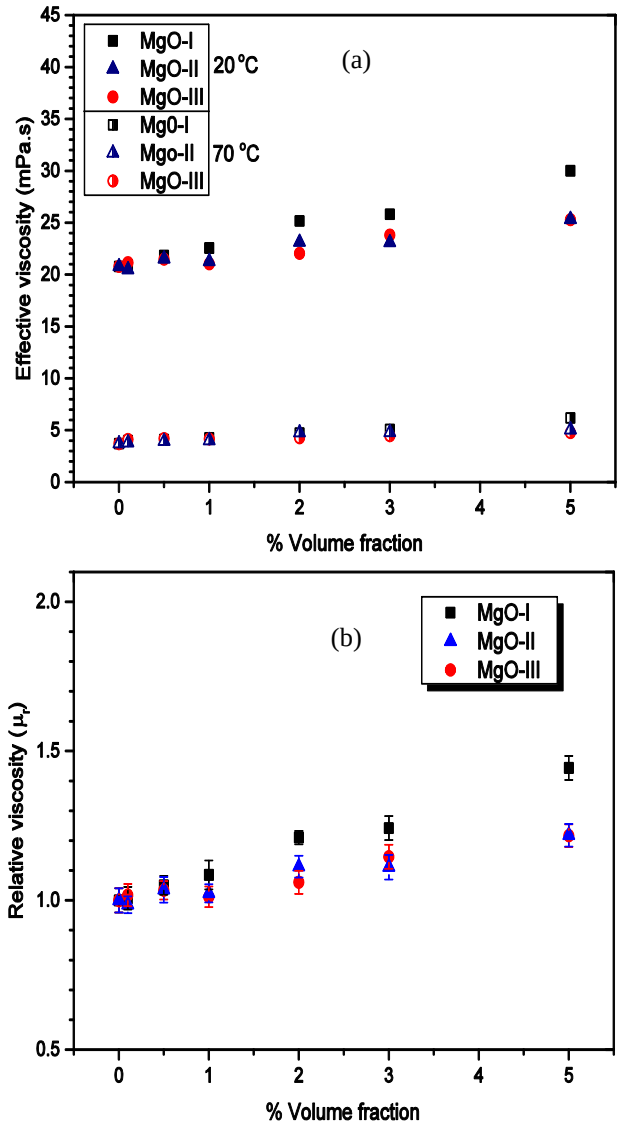
MgO-I
MgO-II
MgO-III
20 °C
Mg0-I
Mgo-II
MgO-III
70 °C
(a)
Effective viscosity (mPa.s)
% Volume fraction
(b)
MgO-I
MgO-II
MgO-III
Relative viscosity (μr)
% Volume fraction

Fig.9

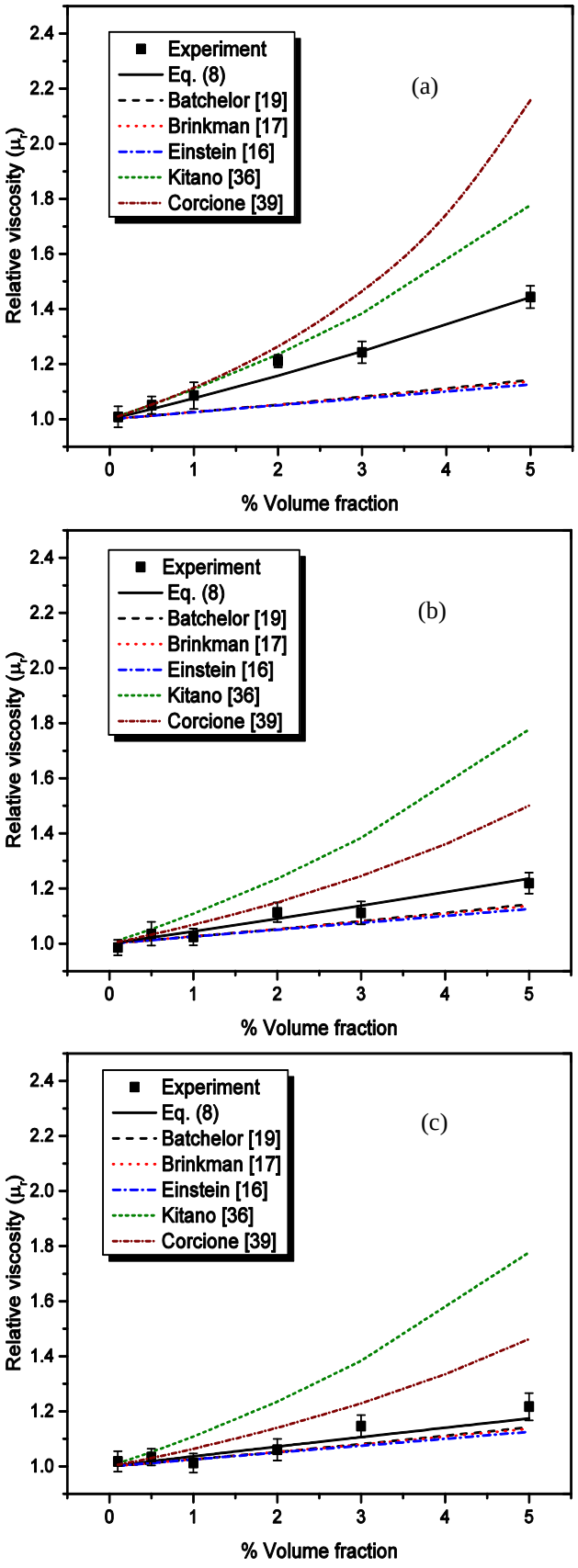
Experiment
Eq. (8)
Batchelor [19]
Brinkman [17]
Einstein [16]
Kitano [36]
Corcione [39]
(a)
(b)
(c)
Relative viscosity (μr)
% Volume fraction
1.0
1.2
1.4
1.6
1.8
2.0
2.2
2.4
0
1
2
3
4
5

Fig. 10

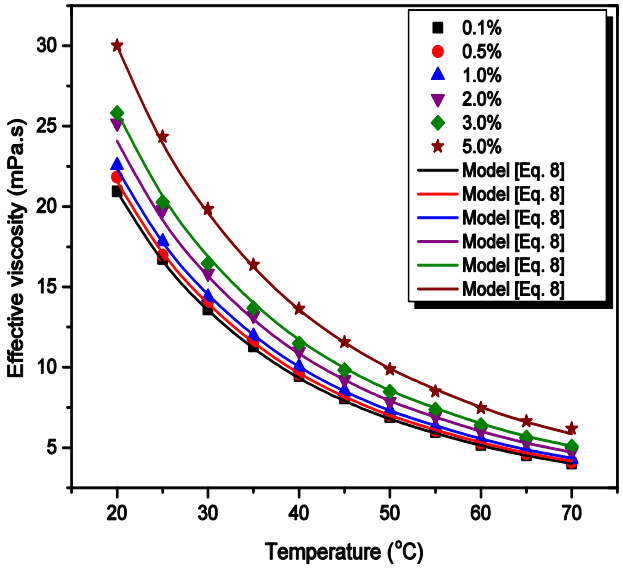
0.1%
0.5%
1.0%
2.0%
3.0%
5.0%
Model [Eq. 8]
Model [Eq. 8]
Model [Eq. 8]
Model [Eq. 8]
Model [Eq. 8]
Model [Eq. 8]
Effective viscosity (mPa.s)
Temperature (°C)
30
25
20
15
10
5
20
30
40
50
60
70

Fig. 11

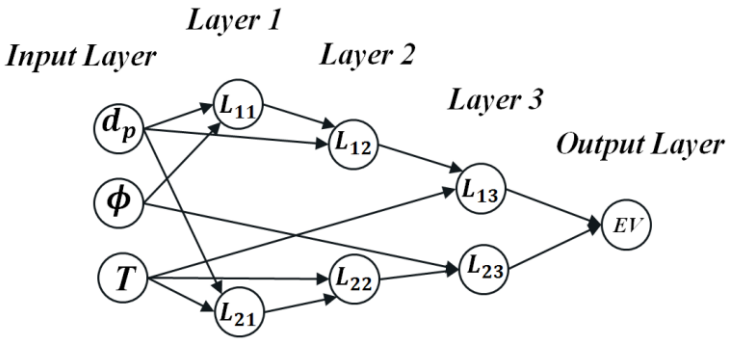
Input Layer
Layer 1
Layer 2
Layer 3
Output Layer
d_p
ϕ
T
L_{11}
L_{12}
L_{13}
L_{21}
L_{22}
L_{23}
EV

Fig. 12

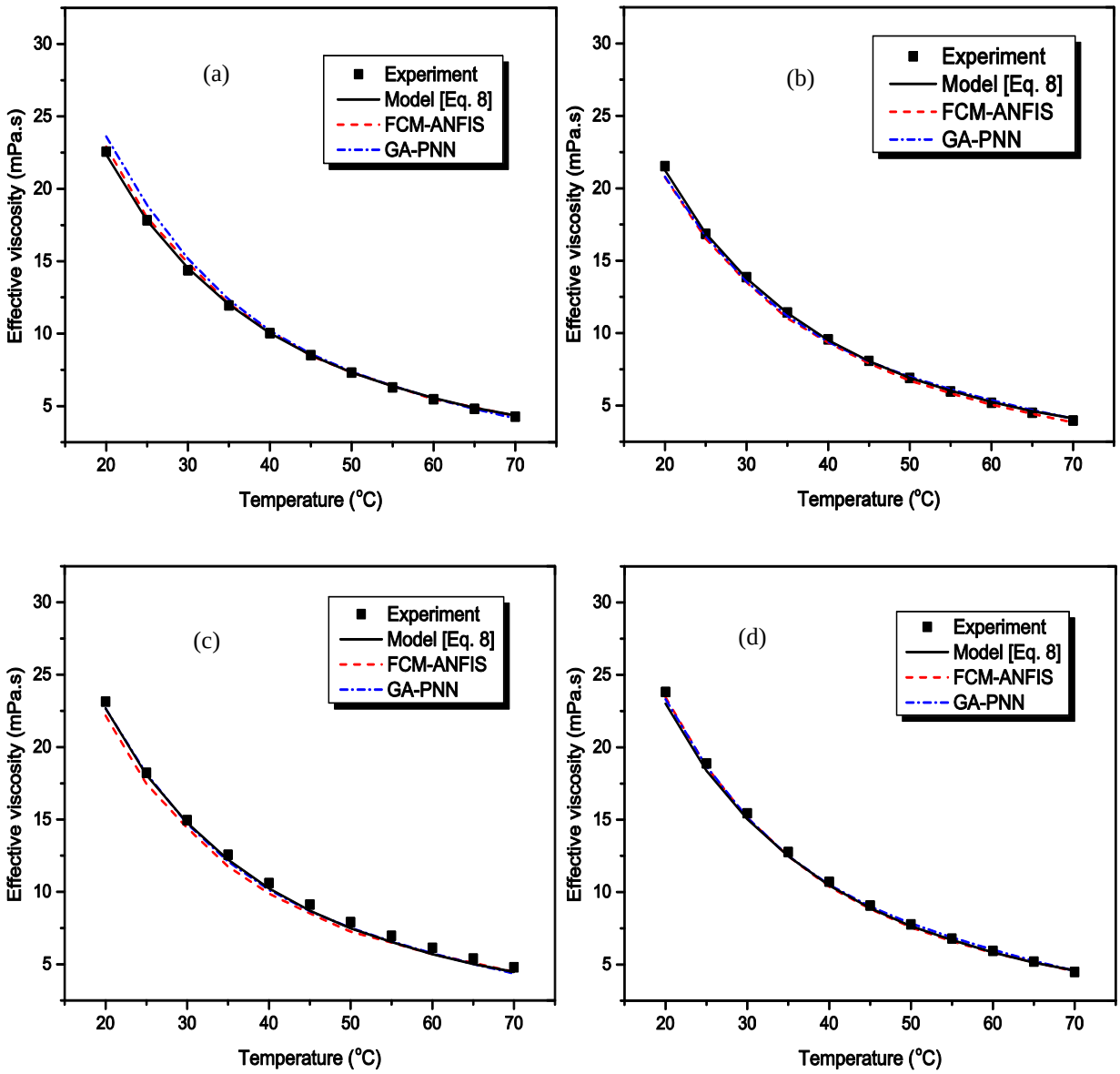
(a)
(b)
(c)
(d)
Experiment
Model [Eq. 8]
FCM-ANFIS
GA-PNN
Effective viscosity (mPa.s)
Temperature (°C)
5
10
15
20
25
30
20
30
40
50
60
70

Fig. 13